1   **Improved Spectral Angle Mapper applications for mangrove classification using SPOT5 imagery**

2   Xiu Su, Xiang Wang *, Jianhua Zhao, Ke Cao, Jianchao Fan, Zhengxian Yang

4   National. Marine Environmental. Monitoring Center, Dalian 116023, China.

6   **Corresponding author**: Xiang Wang, National. Marine Environmental. Monitoring Center, Dalian

7   116023, China.

8   **Tel.**: +8619969339353, **Fax**: +86-0411-84783329, **E-mail:** xwang@nmemc.org.cn

1   **Abstract**

2   The traditional Spectral Angle Mapper (SAM) is an image classification method that uses image

3   endmember spectra. Image spatial structure information may be neglected, especially in mangrove

4   classification research where there is greater spectral similarity between species. This study combined

5   object-oriented classification to improve the accuracy of the method in mangrove ecosystems. A

6   mangrove area in Guangxi's coastal zone was chosen as the study site, and spectral feature analysis and

7   ground investigations were carried out, combining pixel purification, training sample set optimization,

8   and watershed image segmentation algorithm to improve the SAM. The improved SAM was used to

9   classify SPOT5 remote sensing image data for a mangrove ecosystem and then classification accuracy

10   was assessed. The results showed that the improved SAM had better classification accuracy for SPOT5

11   imagery. Accuracy for each mangrove species was greater than 80% and overall accuracy was greater

12   than 90%, which showed that SAM was applicable for mangrove remote sensing. This application

13   potential for classification and information extraction lays the foundation for commercialized remote

14   sensing monitoring of mangrove ecosystems..

16   **Keywords:** Spectral Angle Mapper; mangrove classification; SPOT5 remote sensing image data;

17   Watershed image segmentation algorithm; Training sample set optimization

1   **1. INTRODUCTION**

2   Mangrove forests are tropical and subtropical intertidal wetland woody plant communities

3   predominantly composed of mangrove evergreen trees or shrubs (Fan and Wang, 2017). These

4   ecosystems extend from land to ocean, with particular morphological structure and physiological

5   characteristics. They are of great significance for environmental protection, ecological balance, and

6   biodiversity conservation in coastal zones (Zhang, 2001). Due to global warming, shoreline change,

7   and irresponsible development and destruction, however, mangrove ecosystems have been seriously

8   damaged and their monitoring and protection have become top priorities. Mangrove tidal flats have

9   complex topography, there are numerous estuaries and tidal creeks that are often swampy. Field

10   measurements are very difficult and consume a lot of human and material resources. Remote sensing

11   technology has the advantages of large coverage areas, short data update periods, and high spatial

12   resolutions, and has become the primary means for obtaining mangrove information quickly (Li et al.,

13   2008; Hernández, et al.,2005). Correct understanding of the distribution of mangroves, as well as the

14   location and changes in different mangrove species, are important aspects of mangrove protection and

15   management.

16   Visible satellite remote sensing is the primary data source for mangrove remote sensing

17   classification research, including low- and medium-resolution Landsat TM, Landsat MSS and SPOTXS

18   satellite data (Cao et al.,2011;Zhang,2011), high-resolution IRS and SPOT5/6 data, and sub-meter

19   resolution IKONOS, QuickBird, and WorldView data (Liu et al.,2007;Li and Dai, 2015; Kuenze et

20   al.,2011;Tang et al.,2015). The use of spectral information to classify mangroves, non-mangroves, and

1   individual mangrove species has become an important research topic. The Spectral Angle Mapper

2   (SAM) is a commonly used method for image classification using image endmember spectra. This

3   method can eliminate the influence of illumination and terrain to improve feature recognition. It has

4   been widely applied for ground object calibration (Freek,2006), vegetation research (Zhang et

5   al.,2006), hyperspectral image compression (Qian,2004), and more. However, multi-spectral images

6   also may also contain identical objects with different spectral signatures, and different objects with the

7   same spectral signature. Therefore, using only spectral information for classification can lose spatial

8   information in the high resolution image. This study combined object-oriented classification with a

9   watershed image segmentation algorithm to improve the SAM. A mangrove area on the coast of

10   Guangxi was selected for study. Based on field measurements of mangrove spectral information and

11   the inversion of remote sensing reflectance, mangrove interspecies classification using pansharpening

12   2.5m resolution SPOT5 satellite imagery was performed. The classification results were evaluated for

13   accuracy, providing a scientific basis for remote sensing monitoring of mangrove ecosystems.

14   **2. METHODS**

15   **2.1. SAM**

16   The basic principle of SAM is to distinguish between categories by calculating the Spectral angle

17   between the pixel spectrum and reference spectrum. The test spectrum is the average spectrum of

18   known points extracted from the image, and the reference spectrum is the standard spectrum measured

19   in the field. Spectra are projected as a vector with direction and length onto N-dimensional space. One

20   classification method is according to the angle α between the pixel spectral vector X and the reference

1   spectral vector Y, as shown in Fig. 1.

2   -----------------------------------

3   Insert Figure 1

4   -----------------------------------

6   The SAM formula is as follows:

7        $\cos \alpha = \frac{XY}{|X||Y|}$ (1)

8   Where X is the pixel spectral vector; Y is the reference spectral vector; α is the angle between the

9   spectra, representing the similarity between the spectral vectors, and the smaller α is the closer the X is

10   to Y

11   **2.2. Improved SAM**

12   The traditional SAM first selects training samples, obtains the average value of the training

13   sample spectral vectors, and then classifies them by setting the threshold(Fig2). That is, when the

14   spectral angle between the pixel spectral vector and the average spectral vector of the training sample is

15   less than the set threshold, the pixel and the corresponding sample are considered to belong to the same

16   land type. When a certain land type contains more types of features and the spectral composition is

17   more complicated, however, the average spectral vector has limitations and may not necessarily

18   represent that particular type. Therefore, the training sample set is rationally optimized before

19   classification(Fig.3).

20   -----------------------------------

1   Insert Figure 2

2   ------------------------------------

3   ------------------------------------

4   Insert Figure 3

5   ------------------------------------

7   First, a Minimum Noise Fraction Rotation (MNF ROTATION) was performed on the image data.

8   MNF is proposed and modified by Green(Green et al,1988,), that is essentially a principal component

9   analysis with two overlapping processes. The first transformation is used to separate and readjust the

10   noise in the data, and the second step is the standard principal component transformation of

11   Noise-whitened data. The signal-to-noise ratio is arranged from large to small, thereby overcoming the

12   influence of noise on image quality. It can be seen from the eigenvalue graph (Fig.4) that the

13   eigenvalues of the first three bands were higher, while the fourth band with eigenvalues close to one

14   was mostly noise.

15   ------------------------------------

16   Insert Figure 4

17   ------------------------------------

18   Next, using the Pixel Purity Index (PPI) method, the first three principal components from MNF

19   processing were used as analytical data, and the purest pixel was extracted for various mangrove types

20   in the study area. The PPI was adopted using ENVI 'automated spectral hourglass', that is a new

1   automated procedure in the hyperspectral analysis process (Boardman et al., 1995) for defining

2   potential image endmember spectra (Bateson and Curtiss, 1996) for spectral unmixing (Lillesand and

3   Kiefer, 2000). After PPI processing, the pixels from different types of mangroves displayed different

4   colors in the PPI window. All pixels of the same color were classified together and defined as

5   representative sample point sets. Ground measurements were used to determine the category attribute

6   of each representative sample point set. Finally, the spectral angle set between the vectors of the

7   pixels in the image and all the vectors for various representative sample point sets was calculated.

8   Comparing the spectral angle set , and the category corresponding to the smallest one was selected as

9   the pixel category attribution. In this way, the SAM optimized by the training sample set takes the

10   particularity of ground spectral composition into consideration and improves the accuracy of the

11   classification.

12   The SAM is a pixel-by-pixel classification method, and the results are relatively fragmented.

13   Therefore, combined with object-oriented classification, this paper used trapezoidal high-pass filtering

14   to enhance the SAM results and strengthen the texture information. Then the watershed image

15   segmentation method was used to segment the filtering results. Finally, results were formed using the

16   "watershed segmentation" image method. Its purpose is to divide the image into characteristics regions,

17   that is, extract the edges of the objects in the image, i.e. adjoining pixels with similar gray scale values

18   that reflect the degree of the depth of the image pixel color are connected to each other to form a closed

19   contour(Fig. 5), so that it can be reasonably assumed that all points in the closed contour obtained by

20   the watershed segmentation belong to the same category(Shu Su and Yang Ming,2016). The

1 classification result of mangroves divided by watershed is shown in Fig. 6. This technique can

2 significantly reduce fragmentation and improve image classification accuracy.

3 ------------------------------------

4 Insert Figure 5

5 ------------------------------------

6 Insert Figure 6

7 ------------------------------------

8 **2.3. Data Description**

9 **2.3.1 Overview of the study area**

10   The coastal area of Guangxi is located in the northern part of the Beibu Gulf, in the

11 southwestern-most coastal area of China's 18,000 kilometers of mainland coastline (21°24'N～22°01'N,

12 107°56'E～109°47'E) with Guangdong   to the east . It is bordered by the Ximi River estuary west of

13 the Beilun River estuary on the Sino-Vietnamese border. The Guangxi coastal zone has a northern

14 tropical monsoon climate. The annual average air temperatures range is from 22°C to 23.4°C, the

15 annual average coastal ocean surface temperatures range is from 23.1°C to 23.8°C, and salinity range is

16 from 18 to 31 (Deng and Song,2011). The tidal range in Guangxi is relatively large. The maximum tide

17 tidal range is 7.03 m, the maximum ebb tide tidal range is 6.25 m, and the average tidal range is 2.13 to

18 2.52 m. (Zhang, 2009);. Various types of mangrove populations are found along low tide, mid-tide, and

19 high tide belts (Yang et al,2017).

20 **2.3.2 Sample layout and GCP data collection**

21   On-site field reconnaissance was carried out in the Shankou Mangrove Reserve. According to the

1 purpose of the study and the actual study area, four sections were defined. In each section, a

2 community survey sample was set up along the inner edge of the mangrove, the tidal creek and the

3 outer edge to monitor the dynamics of the mangrove community. A total of 12 sample plots were

4 surveyed. The plots were 10m×10m, and community type, structure, coverage were collected. At the

5 same time, an INVICTA 210 high-precision GPS/beacon two-in-one receiver was used to measure

6 ground spectral data and collect more than 80 ground control points (GCPs) with a positioning

7 accuracy of 1m.

8 **2.3.3 Spectral measurements and processing**

9   A FieldSpec 3 Pro dual-channel field spectrometer produced by American ASD Company was

10 placed at a distance of 1.5 m above the canopy, perpendicularly facing the target object vertically, or at

11 least maintaining an angle between the probe and the normal of the horizontal plane within $\pm 10\,°$. The

12 FieldSpec 3 Pro dual-channel field spectrometer can continuously measure from 350nm to 1050nm.

13 The weather was clear and cloudless, the wind speed was less than 3m/s, and measurements were

14 mainly concentrated   from October 23 to October 27, 2017 between 10:00-14:00. When measuring,

15 shadows were avoided within the field of view of the probe.

16   The study measured spectral data for several mangrove tree species along the Guangxi coast, as

17 well as data for various non-mangroves adjacent to the mangrove populations, to extract mangrove

18 distribution and classification information. Mangrove species measured included *Avicennia*

19 *marina(Am.)*, *Aegiceras corniculatum(Ac.)*, *Kandelia candel(Kc.)*, *Rhizophora stylosa* (*Rs.*), *Bruguiera*

20 *gymnorrhiza(Bg.)*, *Excoecaria agallocha Linn*(*EAL.*), and *Sonneratia apetala*(*Sa.*). Non-mangrove

21 features included *Spartina alterniflora Loisel.*, *Manihot esculenta Crantz*, and mudflats, and a total of

22 76 sample data points were collected.

1   The spectral curve of each measured feature was recorded as Xi, i = 1, 2, 3, ,, 76. Ground object

2   reflectance was calculated using equation (2) (Yu et al.,2006):

$$S_m = \frac{S_t}{S_p} \times R_p$$

3   (2)

4   Where S_m is the reflectance of the ground object; S_t is the measured electrical signal value of the target

5   ground object output from the instrument; S_p is the measured signal value of the diffuse reflection

6   reference plate output from the instrument; R_p is the reference plate reflection obtained by laboratory

7   calibration. After obtaining the ASD spectrometer spectral reflectance for each species on site, band

8   processing of measured Rrs(λ) based on the spectral response function for SPOT5 image data was

9   carried out using the formula:

$$R_{rs}(Bandx) = \frac{\int_{400\mu m}^{1000\mu m} R_{rs}(\lambda) F_s(\lambda) d\lambda}{\int_{400\mu m}^{1000\mu m} F_s(\lambda) S_x(\lambda) d\lambda}$$

10   (3)

11   Where *Rrs(Bandx)* is the reflectance of band *Bandx* from the image sensor; *Rrs(λ)* is the remote sensing

12   reflectance collected by the ASD spectrometer; *Fs(λ)* is the solar irradiance outside the atmosphere at

13   the average distance between the sun and the earth; and *Sx(λ)* is the spectral response function of band

14   *Bandx*.

15   **2.3.4 Satellite data**

16   This study selected six SPOT5 remote sensing image scenes from May to October 2017 with 2.5m

17   panchromatic spatial resolution (0.49~0.69 μm), and four multispectral bands with 10m resolution -

18   including Band1: 0.49~0.61 μm, Band2: 0.61~0.68 μm, Band3: 0.78 ~ 0.89 μm, Band4: 1.58~1.78 μm.

19   The data covered the entire Guangxi coast. Remote sensing image data preprocessing mainly includes

1   satellite data radiation correction, atmospheric correction, orthorectification, and data fusion.

2   **Radiation Correction:** The multispectral image DN values were converted into radiance data

3   using the absolute radiometric scaling factor for the SPOT5 satellite.

4   **Atmospheric correction:** The SPOT5 data were atmospherically corrected using the FLAASH

5   atmospheric correction module in ENVI 5.3 software, and the relevant parameters were input to

6   calculate apparent reflectance data after atmospheric correction.

7   The formula for converting apparent reflectance data into remote sensing reflectance is as follows:

8   $R_{rs} = \rho_w / \pi \tau_o$ (4)

9   $\tau_o = \exp\left(-\tau_r \cos\theta_o / 2\right)$ (5)

10   Where ρ_w is the apparent reflectance; τ_o is the diffuse transmittance of sunlight; τ_r is the Rayleigh optical

11   thickness, which can be calculated according to the theoretical discrete model; and θ_o is the solar zenith

12   angle. As τ_o is very close to 1, for the sake of simplicity, it is typically omitted as a factor.

13   **Orthorectification:** Generally, the RPG file that comes with the image is used to select control

14   points and the SPOT5 sensor model is used to correct it. The total error was controlled within 0.5 cells

15   (a cell is 2.5 m square).

16   **Data fusion:** A pansharpening fusion method for image fusion was used to in this paper. That is

17   the process of integrating a high spatial resolution panchromatic image with a low spatial resolution

18   multispectral image to obtain a multispectral image with high spatial and spectral resolution(Liu et

19   al.,2019). After fusion, the spatial and spectral resolution of the image are improved, and the boundary

20   of the object is more clear.

1   According to the definition of wetlands in the "RAMSAR Convention on Wetlands"(Valencia

2   Rodriguez and I.Dario,2004), combined with the current situation of wetlands in China, the Guangxi

3   Coastal Wetland Research Area (Fig. 7) was defined.

4   ------------------------------------

5   Insert Figure 7

6   ------------------------------------

7   **2.4. Data Analysis**

8   The remote sensing reflectance of mangroves along the Guangxi coast and the SPOT5

9   multispectral band range are shown in Fig. 6. Mangroves had the same spectral curves as other general

10   green plants and exhibited distinct multi-peak and multi-valley characteristics (Xiao et al,2007). There

11   was peak reflectance of green light between 515 nm and 588 nm, and the reflectance was 9% to 10%.

12   The reflectance of the red absorption valley between 610 nm and 678 nm is reduced to 2% to 5%;

13   There is a "red edge" characteristic of increasing reflectance from the red to the near infrared region

14   between 700 nm and 740 nm,, and the reflectance increased from 5% to 20% to 40%;while between

15   750 nm and 1000 nm there was a fluctuating near-infrared high-order platform. Reflectance was

16   maintained at 25% to 55%. However, because the mangrove community is located on the water body

17   and a tidal flat, it had higher heat absorption and lower reflectance than the vegetation on land which is

18   the curve with the highest reflectance between 750 nm and 1000 nm (Fig. 8). This difference was

19   especially clear in the infrared region.

20   ------------------------------------

1   Insert Figure 8

2   -------------------------------------

3   There were minor spectral differences between the various types of mangroves, and the wave

4   patterns and trends of the spectral curves of various mangroves were consistent, and peak-to-valley

5   values appeared in roughly the same bands interval, but there were still some subtle differences. In the

6   Band 1 and 2 range, line height changed little. Reflectance values for *Am* in Band 3 were significantly

7   smaller than that of other mangrove species. *Sa* values were slightly higher than *Am*, but also lower

8   than other mangrove types, and values were roughly in the following order: $R_{Bg} > R_{Eal} > R_{Rs.} > R_{Ac.} >$

9    $R_{Kc.} > R_{Sa.}$.

10   **3. RESULTS**

11   **3.1. Classification Results**

12   Mangrove species in Guangxi were divided into seven categories in this study, *Am.*, *Ac.*, *Kc.*, *Rs.*,

13   *Bg.*, *Eal.*, and *Sa.*. Combining on-site measured spectral data with precise coordinate information for

14   various types of mangrove boundary points and red tree boundary points, the initial sample set for each

15   mangrove was obtained using the Region Of Interest(ROI) tool in ENVI. Then the training sample set

16   was performed using the improved method above. Finally, the improved SAM combined with

17   watershed image segmentation method was implemented in IDL language programming to classify the

18   image. The final classification results are shown in Fig. 9.

19   -------------------------------------

20   Insert Figure 9

1   -----------------------------------

2   **3.2. Accuracy Evaluation**

3   There are many indicators that analyze and evaluate the accuracy of remote sensing

4   classification ,among which the confusion matrix and KAPPA coefficient are the most commonly used.

5   Among them, the confusion matrix can see the type and number of the classification and

6   misclassification of each feature, and the KAPPA coefficient represents the proportion of errors

7   reduction caused by the classification compared to the errors caused by the completely random

8   classification.. The formula is:

9    $$\text{KAPPA} = \frac{N\sum_{i=1}^{r} x_{ii} - \sum_{i=1}^{r}(x_{i+} \times x_{+i})}{N^2 - \sum_{i=1}^{r}(x_{i+} \times x_{+i})} \quad (6)$$

10   Where r is the total number of columns in the error matrix (the total number of categories); x_{ii} is the

11   number of pixels in the i-th row and i-th column of the error matrix (the number of correct

12   classifications); x_{i+} and x_{+i} are the total number of cells in the i-th row and i-th column; and N is the

13   total number of cells used for accuracy evaluation.

14   Using the field survey results of the study area as reference data, 3556 random samples were

15   selected to create the error matrix and the overall accuracy and KAPPA coefficient were calculated.

16   The error matrix for the unmodified spectral angle classification is shown in Tab.1, and the error matrix

17   for the improved SAM is shown in Tab.2.

18   -----------------------------------

19   Insert Table 1

1   -----------------------------------

2   -----------------------------------

3   Insert Table 2

4   -----------------------------------

5   In Tab.1 and 2,each column represents the predicted class, the column total represents the total

6   number of samples predicted for the category; Each row represents a real category data, the row total

7   represents the total number of real sample of the class. Among them, the bold data indicates the number

8   of cells correctly classified, and Accuracy indicates the proportion of samples that are correctly

9   classified. Precision denotes the proportion of Predicted positive cases that are correctly real positives.

10   Recall denotes the proportion of real positive cases that are correctly predicted positive cases by the

11   predicted positive rule(Powers and David,2011). As can be seen ,the improved SAM had higher

12   accuracy indices than the unmodified SAM. The accuracy for each mangrove species was greater than

13   80%, and the overall accuracy was greater than 90%. The KAPPA coefficient was 0.8804, which was

14   greater than the minimum allowable discriminant accuracy of 0.7 (Shi et al.,2000). Compared with

15   other related research (Weng,2006;Liu et al.,2007) based on SPOT5 data and mangrove classification ,

16   the accuracy also improved, which further demonstrated the application and potential of the improved

17   SAM in mangrove classification and information extraction.

18   **4. CONCLUSIONS**

19   In this paper, an image classification method based on pixel purification, training sample set

20   optimization, and an image segmentation algorithm for improving the SAM was used to classify

1 mangrove species in 2.5m resolution SPOT5 satellite images using pansharpeningfusion and covering

2 the entire Guangxi coastal zone. Following atmospheric correction of the SPOT5 image, the remote

3 sensing reflectivity was obtained by inversion. Combined with the measured spectral characteristics of

4 mangroves, the training sample set was selected from the reflectance values and optimized. The

5 classified results underwent post-processing, such as watershed segmentation and statistical merging,

6 before classification accuracy was analyzed. The results showed that, first, the improved SAM

7 combined with training sample set optimization takes the particularity of ground spectral composition

8 into consideration. Combined with the watershed segmentation algorithm, the classification results can

9 be post-processed, which can effectively avoid the fragmentation of the results. Together they can

10 improve the overall classification accuracy. Second, the accuracy of each mangrove type was greater

11 than 80%, and the overall accuracy was greater than 90%. In addition, the KAPPA coefficient was

12 0.8804, which was higher than the minimum allowable discriminant accuracy of 0.7. All of the above

13 findings show that the application value and potential of the improved SAM for the classification of

14 mangrove species provide more rigorous technical support for relevant management departments.

16 **Compliance with Ethical Standards**

17 **Funding:** This study was funded by "National Key R&D Program "Collaborative Research on

18 Global Risk Assessment of Coastal and Coastal Regions" (2017YFA0604902)" and "National Key

19 R&D Program - Marine Target Identification and Monitoring System Integration and Application

20 Demonstration (2017YFC1404900)"

1   **Conflicts of Interest:** They have no conflict of interest.

1 **REFERENCES**

2   1. Bateson A and Curtiss B. A method for manual endmember selection and spectral unmixing.

3   Remote Sensing of Environment, Vol. 55.229-243,1996.

4   2. Boardman JW, Kruse FA and Green RO   Mapping target signatures via partial unmixing

5   of AVIRIS data, In: Summaries of the 5th Annual JPL Airborne Geoscience

6   Workshop,.23-26,1995.

7   3. Cao QX, Xu DP, Pei HB. Biomass Estimation of Five Kinds of Mangrove Community with the

8   KNN Method Based on the Spectral Information and Textural Features of TM Images.

9   Forestry Research, 24(2): 144-150, 2011.

10   4. Deng XM, Song SQ.Current situation and prospects of coastal zone research in Guangxi.Ocean

11   Development and Management,28(7):32-35, 2011.

12   5. Fan HQ,Wang WQ. Some thematic issues for mangrove conservation in China. Journal of

13   Xiamen University(Natural Science) ,56(3):3223-330, 2017.

14   6. Freek V D M. The Effectiveness of Spectral Similarity Measures for the Analysis of

15   Hyperspectral Imagery. International Journal of Applied Earth Observation & Geoinformation,

16   8(1): 3-17, 2006.

17   7. Green A A,Berman M,Switzer P,et al.A transformation for ordering multispectral data in

18   terms of image quality with implications for noise removal［J］.IEEE Transactions on

19   Geoscience and Remote Sensing,26(1) : 65-74,1988.

20   8. Hernández Cornejo R, Koedam N, Ruiz Luna A, et al. Remote sensing and ethnobotanical

21   assessment of the mangrove forest changes in the Navachiste-San Ignacio-Macapule lagoon

22   complex, Sinaloa, Mexico. Ecology & Society , 10(1):16 online,2005.

23   9. Kuenze RC,Bluemel A,Gebhardt S, et al. Remote sensing of mangrove ecosystems: a review.

24   Remote Sensing, 3(5) : 878－928, 2011.

25   10. Li Wei, Cui LJ, Zhang MY, et al. Review of Remote Sensing Technology in Mangrove Wetland

26   Research. Forest Investigation Design , 33(5): 1-7, 2008.

27   11. Li CG, Dai HB. The spatial distribution evolution mechanism of mangroves in Guangxi from

28   1960 to 2010. Chinese Journal of Ecology , 35(18) : 5992-6006, 2015.

29   12. Lillesand TM and Kiefer RW. Remote sensing and image interpretation, 4th Edition, John Wiley

30   &Sons, Inc., New York, 178-198, 2000. Shi PJ, Chen Jin, PAN YH. Analysis on land use

31   change mechanism in Shenzhen ,Acta Geographica Sinica, 55(2): 47-50, 151-160, 2000.

32   13. Liu JM, Ma Jing, Fei RR , et al. Enhanced Back-Projection as Postprocessing for Pansharpening,

33   Remote Sens. 11(6), 712, 2019; https://doi.org/10.3390/rs11060712.

34   14. Liu ZG, Li Jing, Lim BL, et al. Object-based Classification for Mangrove with VHR Remotely

35   Sensed Image. Proc. SPIE ,6752(3):83-87, 2007.

36   15. Powers, David .M.W. Evaluation: From Precision, Recall and F-Measure to Roc, Informedness,

37   Markedness & Correlation. Journal of Machine Learning Technologies, 2, 37-63, 2011.

38   16. Qian S. Hyperspectral Data Compression Using a Fast Vector Quantization Algorithm.

39   Geoscience and Remote Sensing, IEEE Transactions on , 42(8): 1791-1798, 2004.

17. Shu Su,Yang Ming. Hyperspectral Image Classification Method Based on Watershed
    Segmentation and Sparse Representation.Computer Science, 43(2):89-94,2016.

18. Tang HL, Liu Kai, Zhu YH, et al. Classification of mangrove community based on WorldView-2
    data and support vector machine. Journal of Sun Yat Sen University(Natural Science), 54(4) :
    102-111, 2015.

19. Valencia Rodriguez, I.Dario . The Ramsar Convention and waterbirds in the Neotropics La
    convencion de Ramsar y las aves acuaticas en el neotropico , Ornitologia Neotropical, 15:
    445-454 ,2004.

20. Wang HY, Dong GJ, Tang HS, et al. Study on classification technology of coastal hyperspectral
    imagery. Marine mapping ,24(6):20-23.15, 2004.

21. Weng Qiang. Spectral characteristics of mangrove plants and remote sensing image
    classification of mangrove plants. Journal of Xiamen University(Natural Science) , 2006.

22. Xiao HY, Zeng Hui, Yan QJ, et al. Extraction of mangrove community type information based
    on hyperspectral data and expert decision making method. Journal of Remote
    Sensing ,11(4):531-537, 2007.

23. Yang SC, Lu WX, Zou Z, et al. Mangrove wetlands: Distribution, species composition and
    protection in China. Subtropical Plant Science ,46(4):301-310, 2017.

24. Yu Xiang, Zhao DZ, Zhang FS. Hyperspectral Analysis of Mangroves. Journal of Binzhou
    University , 22(6): 53-56, 2006.

25. Zhang GH. Analysis of tidal characteristics in coastal areas of Guangxi［J］. PEARL
    RIVER,1:29-30,2009.

26. Zhang J, Rivard B, S ánchez-Azofeifa A, et al. Intra- and Inter-class Spectral Variability of
    Tropical Tree Species at La Selva, Costa Rica: Implications for Species Identification Using
    HYDICE Imagery. Remote Sensing of Environment,105(2): 129-141, 2006.

27. Zhang QM, Sui SZ. Mangrove Wetland Resources and Their Protection in China. Journal of
    Natural Resources, 16(1): 28-36, 2001.

28. Zhang XH. Extraction of Mangrove Remote Sensing Information Based on Knowledge and
    Rules. Journal of Nanjing University of Information Science & Technology(Natural Science
    Edition) , 3(4): 341-345, 2011.

1 **Tables**

2 **Table 1. Error matrix for the original classification results**

Types	Am.	Bg.	Rs.	Ac.	EaL.	Kc.	Sa.	Total	Recall (%)
Am	**356**	31	29	28	22	26	20	512	69.5
Bg	12	**385**	20	13	5	21	18	474	81.2
Rs	38	21	**386**	43	35	27	32	582	66.3
Ac	25	21	16	**403**	10	21	18	514	78.4
EaL.	55	21	17	19	**315**	22	18	467	67.5
Kc.	11	0	23	32	10	**350**	19	445	78.7
Sa.	37	27	26	12	20	33	**407**	562	72.4
Total	534	506	517	550	417	500	532	3556	
Precision (%)	66.7	76.1	77.4	73.27	75.56	70	76.65		

Overall accuracy =2602÷3556×100%=73.17%   KAPPA=0.6868

4
5

7 **Table 2. Error matrix for the improved classification results**

Types	Am.	Bg.	Rs.	Ac.	EaL.	Kc.	Sa.	total	Recall (%)
Am	**484**	0	0	15	0	22	16	537	90.1
Bg	0	**451**	17	0	3	0	16	487	92.6
Rs	0	15	**474**	11	13	17	0	530	89.4
Ac	20	10	7	**493**	0	12	11	553	89.2
EaL.	11	17	0	7	**388**	0	8	431	90.0
Kc.	8	0	15	15	0	**449**	13	500	89.8
Sa.	11	13	4	9	13	0	**468**	518	90.3
total	534	506	517	550	417	500	532	3556	
Precision (%)	90.6	89.1	91.7	89.6	93.0	89.8	88.0	3556	

Overall accuracy =3207÷3556×100%=90.2%   KAPPA=0.8854

1   **Figure legends**

3   **Fig 1** SAM schematic diagram
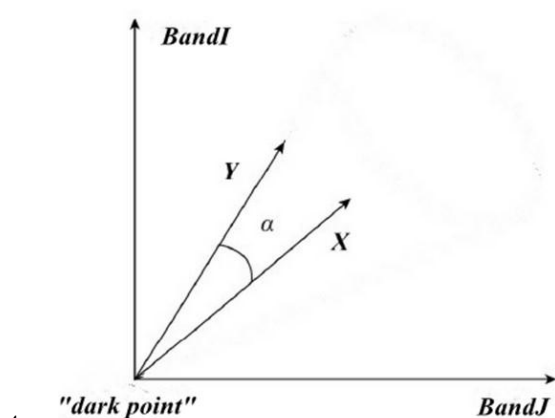
5   **Fig.2 Basic process of SAM**
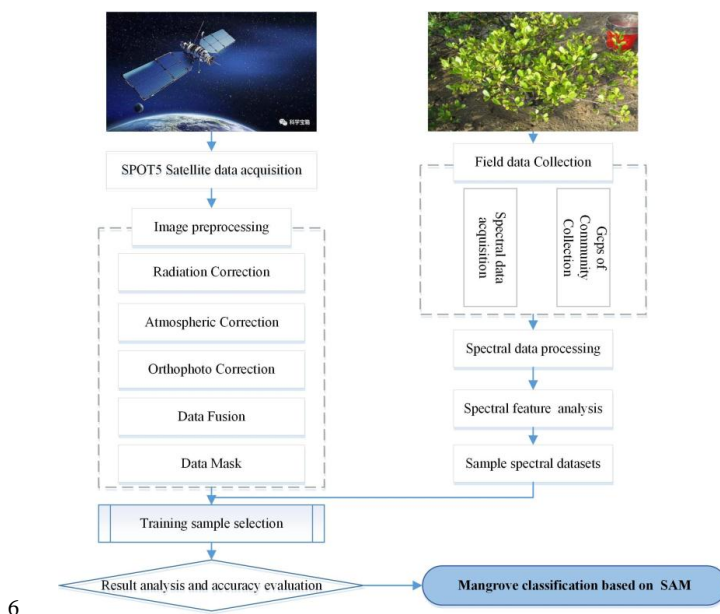
1   **Fig.3 Basic process of Improved SAM**
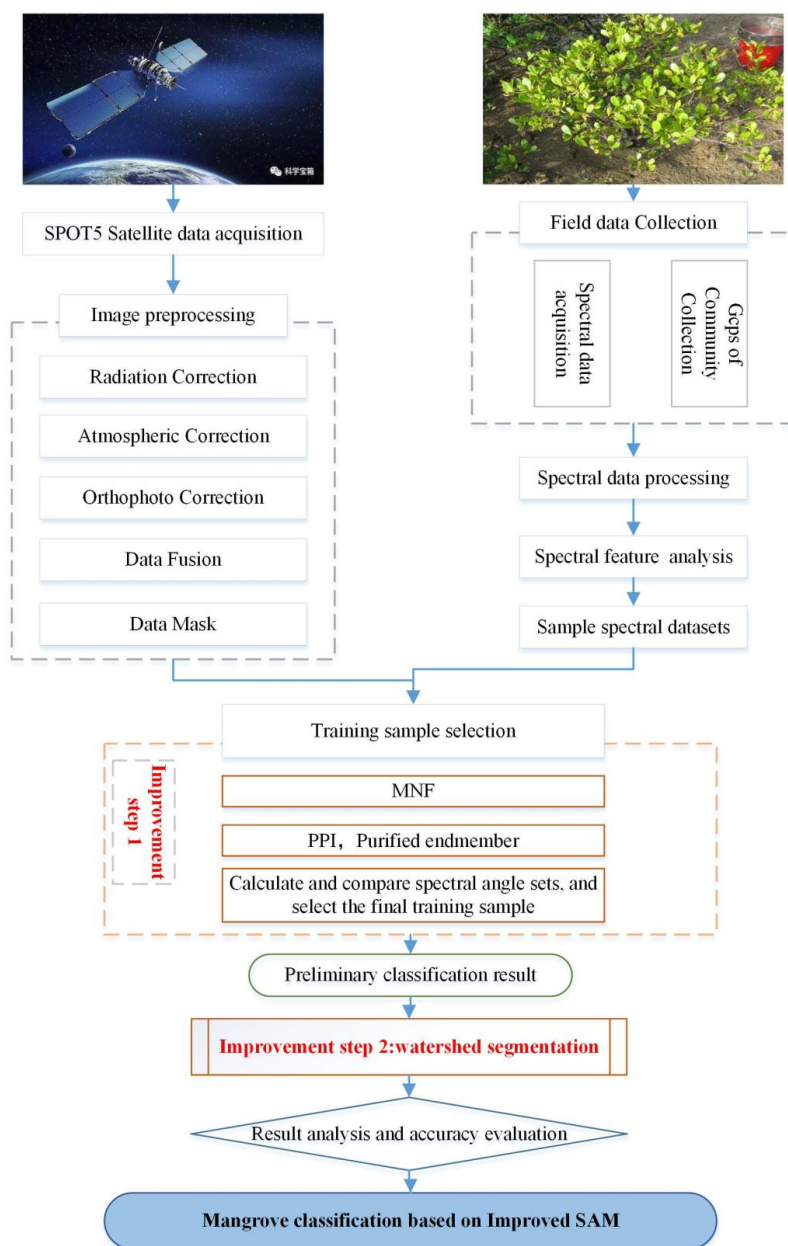
1   **Fig 4 MNF eigenvalue curve**
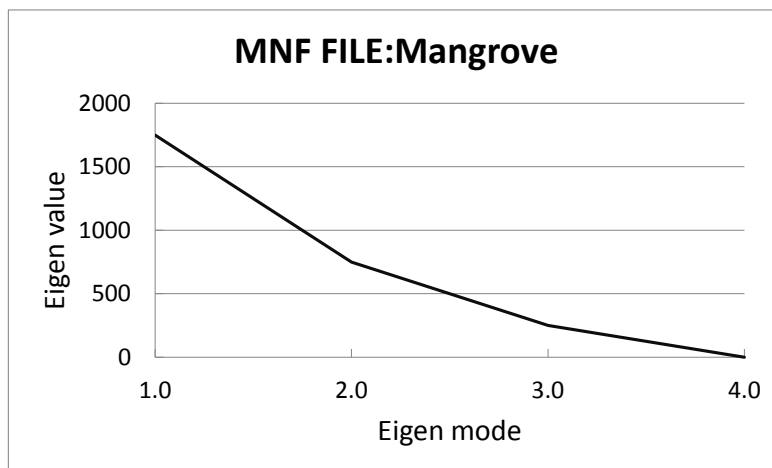
6   **Fig 5 Schematic diagram of watershed image segmentation**

7   **(A)Image showing the internal markers(Minima) and Watershed Line (B)Results of watershed**

8   **image segmentation**
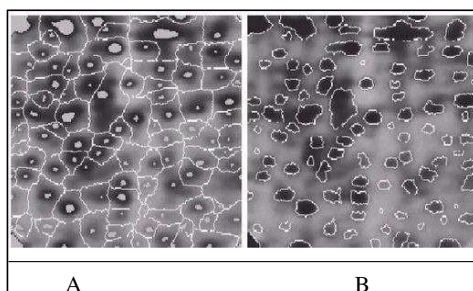
2 **Fig 6 The results of the improved SAM using the watershed segmentation algorithm**

3 (A) SAM (B) Final classification results
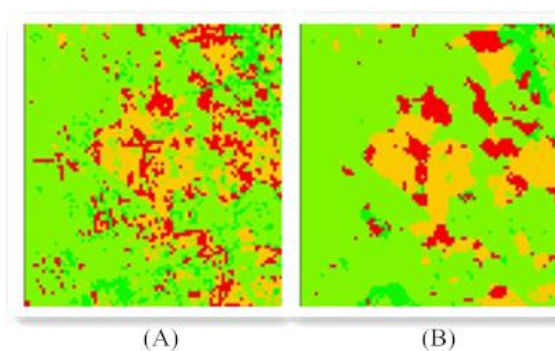
5 **Fig 7 Map of the study area**
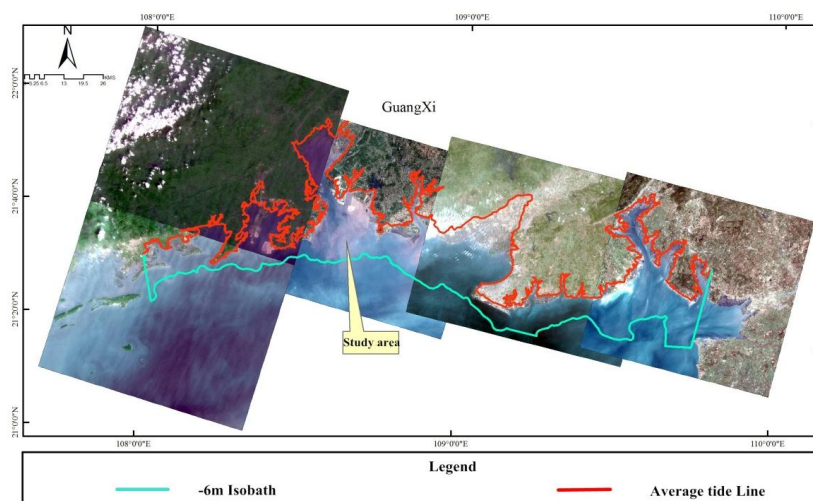
1 **Fig 8 Field spectral reflectance curves for mangroves along the Guangxi coast, and the**

2 **SPOT5 multispectral band range**
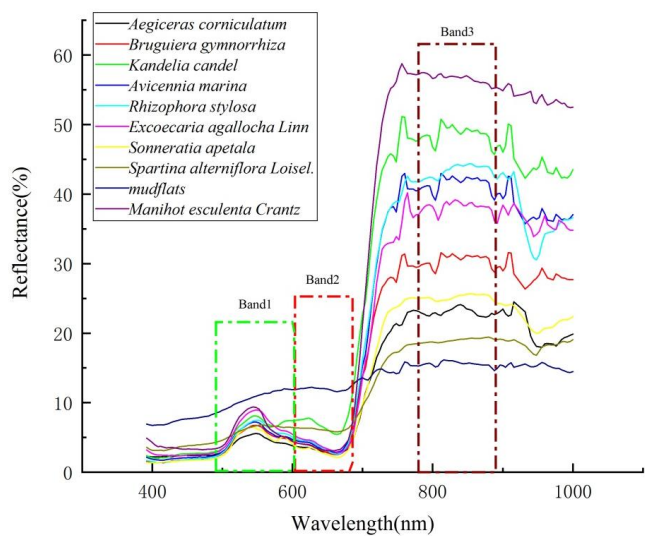
4 **Fig 9 Guangxi mangrove classification map**